Macromolecules

Note

pubs.acs.org/Macromolecules

Poly(methyl methacrylate)-*block*-poly(*n*-butyl methacrylate) Diblock Copolymer Micelles in an Ionic Liquid: Scaling of Core and Corona Size with Core Block Length

Yuanchi Ma[†] and Timothy P. Lodge*[,†,‡]

[†]Department of Chemistry and [‡]Department of Chemical Engineering and Materials Science, University of Minnesota, Minneapolis, Minnesota 55455, United States

Supporting Information

ABSTRACT: The structure of poly(methyl methacrylate)-*block*-poly(*n*-butyl methacrylate) (PMMA-*b*-PnBMA) micelles in the room temperature ionic liquid 1-ethyl-3-methylimidazolium bis(trifluoromethylsulfonyl)imide ([EMIM][TFSI]), a selective solvent for the PMMA block, has been studied using dynamic light scattering (DLS) and small-angle X-ray scattering (SAXS). A series of seven PMMA-*b*-PnBMA diblock copolymers were prepared by reversible addition−fragmentation chain-transfer (RAFT) polymerization, in which the degree of polymerization of the PMMA block was kept constant while the PnBMA block length was varied. All the polymers formed spherical micelles at ambient temperature in dilute solution; their hydrodynamic radius (R_h) and core radius (R_c) were obtained by DLS and SAXS, respectively. It was found that R_c and the degree of polymerization of the core block, N_B, followed a power law relationship in which $R_c \sim N_B^{0.71\pm0.01}$. The corona thickness ($L_{corona}$), given by the difference of R_h and R_c, does not show any apparent dependence on N_B. These results were compared to scaling theory, and were found to be only in partial agreement with the star model proposed by Halperin et al. However, the mean-field calculations of micellar dimensions by Nagarajan and Ganesh were in excellent agreement with the data. This comprehensive experimental study provides precise quantification of the R_c and L_{corona} dependence on core block lengths, due to the use of seven different block copolymers with identical corona block lengths.

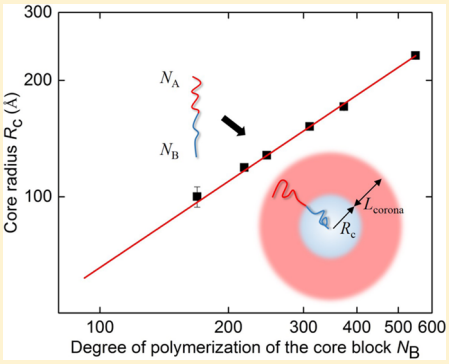

INTRODUCTION

Like small molecule surfactants, A−B diblock copolymers can self-assemble into micellar structures in a selective solvent, with the insoluble B blocks forming the core, surrounded by the solvophilic A blocks as the corona. The structure of spherical micelles can be characterized by the aggregation number (N_{agg}), core radius (R_c), and corona thickness (L_{corona}). A long-standing issue is whether or not there is a universal relationship between these parameters and the degrees of polymerization of the two blocks, N_A and N_B. In order to address this question, many theories have been proposed.[1−13] In the pioneering work of de Gennes,[1] Zhulina and Birshtein,[6] and Halperin and co-workers,[7,8] scaling analysis was applied to a single micelle, in which the total free energy per chain, F, can be written as $F = F_{interface} + F_A + F_B$. The first term accounts for the free energy of the core−corona interface; the second and the third terms are the free energy contributions of the corona and the core blocks, respectively. Subsequently, the total F is minimized to give the dependence of R_c and N_{agg} on N_A and N_B. Notably, Halperin et al. divided micelles into two limiting cases: "hairy" micelles ($N_A \gg N_B$) and "crew-cut" micelles ($N_A \ll N_B$). By omitting F_B in the former case and F_A in the latter, they found that $N_{agg} \sim N_B^{4/5}$ and $R_c \sim N_B^{3/5}$ in the case of hairy micelles, while $N_{agg} \sim N_B$ and $R_c \sim N_B^{2/3}$ in the case of crew-cut micelle.[8] In general, all scaling models suggested that $N_{agg} \sim N_B^{\nu}$ and $R_c \sim N_B^{(1+\nu)/3}$, with $\nu = 0.5-1$, under the assumption that the core is devoid of solvent.

Compared with scaling theory, mean-field theory enables a numerical approach, and can also take into account the three relevant Flory−Huggins parameters χ_{AB}, χ_{AS}, and χ_{BS}, where the subscript S stands for solvent. Leibler, Orland, and Wheeler[3] and Noolandi and Hong[4,5] separately developed models, which were later elaborated by Nagarajan and Ganesh,[9,10] who provided a numerical dependence of N_{agg} on the corona block length, N_A, in contrast to the prediction by scaling models that N_{agg} depends only on N_B. Other detailed approaches, such as Monte Carlo simulation and other computational methods, are also available.[11−13] Extensive reviews in this field can be found elsewhere.[14,15]

In order to test aspects of these theories, many block copolymer/selective solvent systems have been studied using light (static and dynamic) and small-angle (X-ray and neutron) scattering techniques.[16−36] However, most of these studies are not completely quantitative, in terms of testing predictions. Several factors contribute to this. First, the core block should have a low glass transition temperature (T_g), to avoid forming

Received: February 10, 2016
Revised: April 15, 2016

ACS Publications © XXXX American Chemical Society

DOI: 10.1021/acs.macromol.6b00315
Macromolecules XXXX, XXX, XXX−XXX

Table 1. Characteristics of PMMA-*b*-PnBMA Diblock Copolymers

	PMMA block M_n (kg/mol)[a]	PnBMA block M_n (kg/mol)[b]	N_{PMMA}[c]	N_{PnBMA}[d]	Đ
PMMA (25)	25	–	250	–	1.04
PMMA-*b*-PnBMA (25–13)	25	13	250	92	1.04
PMMA-*b*-PnBMA (25–24)	25	24	250	169	1.04
PMMA-*b*-PnBMA (25–31)	25	31	250	218	1.05
PMMA-*b*-PnBMA (25–35)	25	35	250	246	1.05
PMMA-*b*-PnBMA (25–44)	25	44	250	310	1.07
PMMA-*b*-PnBMA (25–53)	25	53	250	373	1.07
PMMA-*b*-PnBMA (25–78)	25	78	250	549	1.11

[a]Number-average molecular weight of the PMMA block was determined by light scattering detection during SEC, with 0.084 mL/g used as the d*n*/d*c* of PMMA.[39] [b]Number-average molecular weight of PnBMA block determined by ^{1}H NMR spectroscopy. [c]Degree of polymerization of PMMA block. [d]Degree of polymerization of PnBMA block.

kinetically frozen cores at the experimental temperature, thereby hindering access to thermodynamic equilibrium. Second, the Flory–Huggins parameter χ between the core block and the solvent should be large enough so that the core is not swollen appreciably. Third, the block copolymer should preferentially form simple spherical micelles, with no larger aggregates. Fourth, many studies use static light scattering to determine the molecular weight of the micelle, and thus to calculate N_{agg} and R_c; in particular for the core radius, this is an indirect method and may be less reliable compared with direct structural techniques, such as SAXS, SANS, and transmission electron microscopy (TEM).

In this report, poly(methyl methacrylate)-*block*-poly(*n*-butyl methacrylate) (PMMA-*b*-PnBMA) in the ionic liquid 1-ethyl-3-methylimidazolium bis(trifluoromethylsulfonyl)imide ([EMIM][TFSI]), which features a lower critical solution temperature (LCST), was selected as the model system, as it possesses particularly favorable attributes: (*i*) ease of synthesis and molecular weight control; (*ii*) low T_g of the core block (the T_g of PnBMA is ∼20 °C),[37] which avoids the kinetically trapped state of a frozen micelle core; (*iii*) reasonably strong segregation of PnBMA and [EMIM][TFSI]; (*iv*) no evidence of micelle clusters, in contrast to some systems.[20,21] This choice of block copolymer and solvent also provides a wide composition window to study the micelle structure parameters as a function of N_A and N_B. This study with seven samples, all with an identical corona-forming block, should serve as a rigorous test for theory.

■ EXPERIMENTAL SECTION

Materials. PMMA-*b*-PnBMA diblock copolymers were synthesized by sequential RAFT polymerization of methyl methacrylate and *n*-butyl methacrylate, respectively. The ionic liquid [EMIM][TFSI] was synthesized using a procedure adapted from literature.[38] All other reagents were purchased from Sigma-Aldrich and used as received unless otherwise specified. A typical synthesis procedure of PMMA-*b*-PnBMA follows.

Synthesis of PMMA. 4-Cyano-4-[(dodecylsulfanylthiocarbonyl)-sulfanyl]pentanoic acid (CTAC12CN, 0.21 g, 0.52 mmol), methyl methacrylate (MMA, 21 g, 210 mmol) and 4,4′-azobis(4-cyanovaleric acid) (V501, 16.0 mg, 0.057 mmol) were combined with 60 mL of dioxane in a 250 mL Schlenk flask. The flask was sealed by a rubber septum and subsequently subjected to three freeze–pump–thaw cycles to remove oxygen. The flask was then filled with argon, and the reaction was allowed to proceed for 12 h at 80 °C. The product was directly precipitated into hexanes and collected via filtration.

Synthesis of PMMA-*b*-PnBMA. PMMA-CTAC12CN (0.70 g, 0.028 mmol), *n*-butyl methacrylate (*n*-BMA, 0.94 g, 6.6 mmol), and V501 (0.8 mg, 0.0028 mmol) were combined with 7 mL of dioxane in a 100 mL Schlenk flask. The reaction mixture went through three freeze–pump–thaw cycles and was then heated to 80 °C under argon. The reaction was allowed to proceed for 22 h. The resulting copolymer was recovered by precipitation into cold methanol.

The polymers were characterized by size exclusion chromatography (SEC) with a multiangle laser light scattering detector (Wyatt DAWN) and by ^{1}H-nuclear magnetic resonance spectroscopy (^{1}H NMR, Varian Inova 500). The number-average molecular weight (M_n) and dispersity (Đ) of PMMA, as well as the dispersity of the diblocks, were determined by SEC, in which 0.084 mL/g and 0.068 mL/g were used as the d*n*/d*c* for PMMA and PnBMA in THF, respectively. ^{1}H NMR spectroscopy was used to determine M_n of the PnBMA blocks on the basis of the integration ratio between the $-OCH_3$ peak (δ = 3.60 ppm) of PMMA and $-OCH_2-$ peak (δ = 3.95 ppm) of PnBMA (see Figure S1 in the Supporting Information). The characterization results of the seven PMMA-*b*-PnBMA diblock copolymers as well as the PMMA homopolymer are shown in Table 1. The numbers in the brackets refer to the molecular weight of each block in kg/mol.

Preparation of Micelle Solutions. Methylene chloride was used as a cosolvent to dissolve PMMA-*b*-PnBMA; this solution was combined with [EMIM][TFSI] at room temperature in a predetermined ratio, and then purged with nitrogen overnight to slowly remove the cosolvent. The resulting solution was dried at 50 °C under vacuum (<100 mTorr) for at least 12 h prior to use.

Dynamic Light Scattering (DLS). Dynamic light scattering was used to determine the mean and distribution of the hydrodynamic radius (R_h) of the micelles. The micelle solutions were filtered through 0.2 μm filters, and the DLS tubes were flame-sealed to avoid contact with moisture in air. The samples were measured on a home-built spectrometer, as described elsewhere.[34] The normalized intensity autocorrelation function, $g^{(2)}(t)$, was typically obtained at 90°, then treated by inverse Laplace transform using the regularized positive exponential sum (REPES) method to obtain the R_h distribution.[40] Most micelle solutions exhibited a monomodal distribution of R_h, and thus cumulant fitting was used to determine the average decay rate ($\bar{\Gamma}$) and the second cumulant (μ_2)

$$g^{(2)}(t) = 1 + \beta |g^{(1)}(t)|^2 \tag{1}$$

$$\ln|g^{(1)}(t)| = (-\bar{\Gamma}t)\left(1 + \frac{\mu_2 t^2}{2!} - \frac{\mu_3 t^3}{3!} + \dots\right) \tag{2}$$

in which $\mu_2/\bar{\Gamma}^2$ represents the width of distribution.[41] The $\bar{\Gamma}$ obtained from the fitting can be directly related to $\bar{R}_h$ by

$$\bar{R}_h = \frac{kT}{6\pi\eta_s D_0} = \frac{kTq^2}{6\pi\eta_s \bar{\Gamma}} \tag{3}$$

where k, T, η_s, and q are the Boltzmann constant, temperature, solvent viscosity and scattering vector, respectively.

Small-Angle X-ray Scattering (SAXS). Small-angle X-ray scattering was conducted on the 5ID-D beamline of the DuPont–Northwestern–Dow Collaborative Access Team (DND-CAT) at the Advanced Photon Source, Argonne National Laboratory. The beam

DOI: 10.1021/acs.macromol.6b00315
Macromolecules XXXX, XXX, XXX–XXX

energy used was 9 keV, corresponding to a wavelength of 1.38 Å. 2D-SAXS images were collected using a MAR-CCD detector, with the sample-to-detector distance of 5.47 m. Temperature was controlled by an electric heater. Quartz capillary tubes were used for more dilute samples (<10 wt %); aluminum pans were used for the samples with larger concentrations. The samples were annealed at the designated temperature for at least 5 min before exposure to the beam. A typical duration of beam exposure was 10−30 s. The 2D-SAXS images were averaged azimuthally to give one-dimensional $I(q)$ vs q profiles using the data reduction software provided by Argonne National Lab (FIT2D). Subsequently, the solvent background was subtracted from the 1D data, and the resulting intensity profiles were analyzed using a fitting model[42] built in Igor Pro (see Appendix).

RESULTS AND DISCUSSION

Dynamic Light Scattering. The hydrodynamic radius distributions of the seven PMMA-*b*-PnBMA copolymers in [EMIM][TFSI] at 60 °C are shown in Figure 1. The copolymer micelle solutions were prepared with 1 wt % polymer, using the cosolvent method described in the previous section. As can be seen in Figure 1, all the block copolymers form micelles with a very narrow R_h distribution, except for PMMA-*b*-PnBMA (25−13). This exception can be attributed to the short PnBMA block in PMMA-*b*-PnBMA (25−13), which inhibits complete micellization; as is evident in Figure 1a, there is a peak at $R_h \approx 3$ nm, indicating the coexistence of some PMMA-*b*-PnBMA (25−13) free chains at the experimental temperature. The results of the cumulant fitting are summarized in Table 2. These R_h distributions do not show appreciable temperature dependence from room temperature to 100 °C; the DLS results of PMMA-*b*-PnBMA (25−35) at different temperatures are given in Supporting Information as an example (Figure S4).

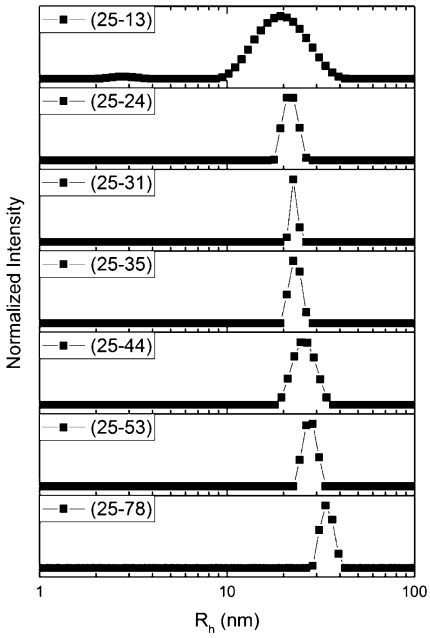

Figure 1. R_h distributions of PMMA-*b*-PnBMA copolymer micelles in [EMIM][TFSI] at 60 °C.

Small Angle X-ray Scattering. In order to determine the core radius (R_c) of the PMMA-*b*-PnBMA block copolymer micelles precisely, SAXS measurements were conducted on these micelle solutions and the scattering profiles fitted to the model developed by Pedersen et al.[42,43] Figure 2 displays the SAXS patterns for all seven PMMA-*b*-PnBMA copolymers in 1 wt % solution at 60 °C. The SAXS data of these micelles also show little temperature dependence, consistent with the DLS results. The SAXS data of PMMA-*b*-PnBMA (25−35) at different temperatures are provided in Supporting Information as an example (Figure S5).

Table 2. Characteristics of PMMA-*b*-PnBMA Micelles in [EMIM][TFSI] by DLS

polymer	average R_h (nm)	$\mu_2/\bar{\Gamma}^2$
PMMA-*b*-PnBMA (25−13)	$17._8$	0.18
PMMA-*b*-PnBMA (25−24)	$22._1$	0.04
PMMA-*b*-PnBMA (25−31)	$22._8$	≈0
PMMA-*b*-PnBMA (25−35)	$24._0$	0.03
PMMA-*b*-PnBMA (25−44)	$26._0$	0.04
PMMA-*b*-PnBMA (25−53)	$27._9$	≈0
PMMA-*b*-PnBMA (25−78)	$34._6$	≈0

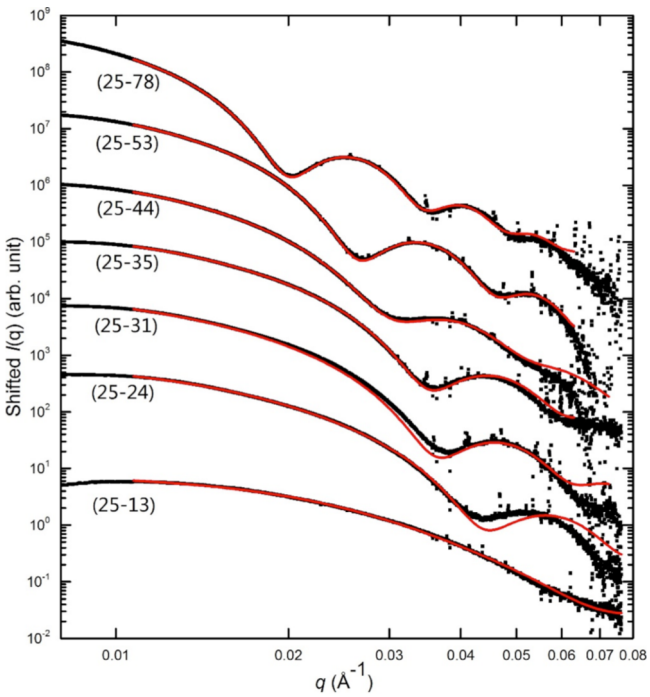

Figure 2. SAXS profiles of PMMA-*b*-PnBMA block copolymer micelles (1 wt %) in [EMIM][TFSI] at 60 °C. The solid lines are best fits to the Pedersen model. The profiles are shifted vertically by factors of 10 for clarity.

As can be seen in Figure 2, the scattering profiles for the six largest polymers show a clear first minimum, which progressively shifts toward lower q as the core block length increases. The only exception is PMMA-*b*-PnBMA(25−13), for which the first minimum approaches the upper limit of the q range used, and is also smeared by the broad R_c distribution as well. The solid curves in Figure 2 represent best fits to the Pedersen model (summarized in the Appendix). The total scattering intensity has contributions from both the core and the corona (as well as the cross-term) (eq A1), but the scattering pattern is still dominated by the core. Consequently, the parameters related to the corona domain, i.e., R_g, a_1 and s, are less reliable than those related to the core (R_c and σ_R). The aggregation number, N_{agg}, is defined as $N_{agg} = 4\pi R_c^3/3v_{core\text{-}block}$ assuming the core is devoid of solvent, as will be discussed subsequently. Furthermore, in dilute solution where the

DOI: 10.1021/acs.macromol.6b00315
Macromolecules XXXX, XXX, XXX−XXX

Table 3. Summary of SAXS Fitting

	R_c (Å)	σ_R (Å)	N_{agg} [a]
PMMA-*b*-PnBMA (25−13)	$58 \pm 2 \times 10^2$	$5 \pm 2 \times 10^2$	$41 \pm 4 \times 10^2$
PMMA-*b*-PnBMA (25−24)	100 ± 6	6 ± 5	112 ± 20
PMMA-*b*-PnBMA (25−31)	119 ± 2	9 ± 4	147 ± 7
PMMA-*b*-PnBMA (25−35)	128 ± 1	10 ± 2	162 ± 4
PMMA-*b*-PnBMA (25−44)	152 ± 1	18 ± 1	215 ± 1
PMMA-*b*-PnBMA (25−53)	171 ± 1	14 ± 1	255 ± 2
PMMA-*b*-PnBMA (25−78)	232 ± 1	22 ± 1	432 ± 2

[a] N_{agg} is calculated by $N_{agg} = 4\pi R_c^3/3v_{core\text{-}block}$, which represents the upper bound of the aggregation number as it assumes the core is only composed of polymer.

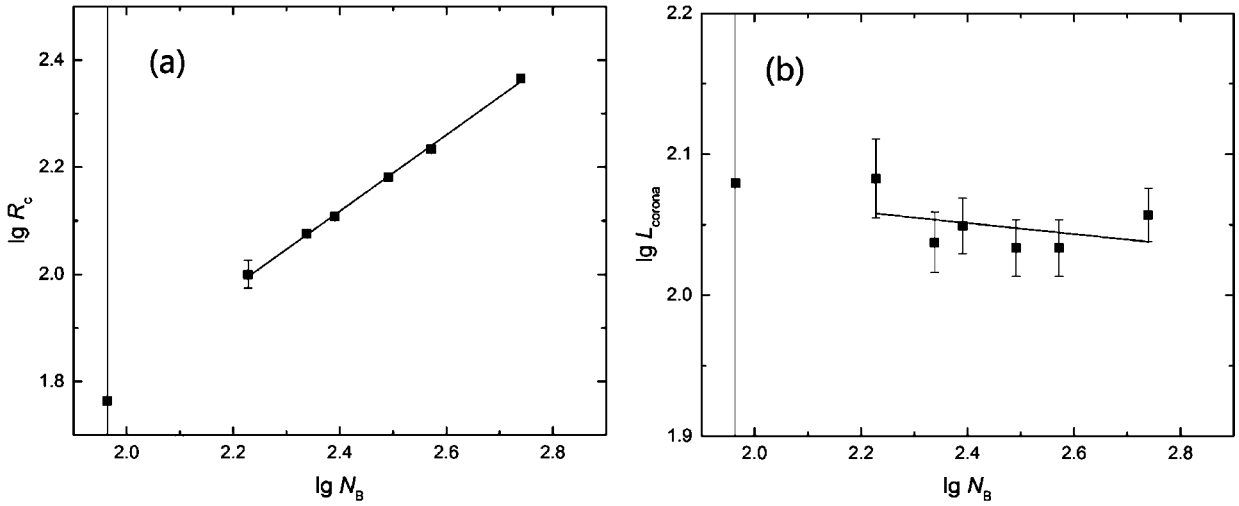

Figure 3. Dependence of (a) the core radius and (b) the corona thickness on the number of repeating units in the core block.

concentration of micelles is significantly smaller than the critical overlap concentration, the structure factor can be neglected, i.e., $S(q) \approx 1$; therefore, the independent parameters that can be accurately obtained from the fitting are the average core radius (R_c) and the standard deviation of the core radius (σ_R). The fitting results are summarized in Table 3. The error in R_c (and thus N_{agg}) for PMMA-*b*-PnBMA (25−13) is much larger than that of the other samples; this is a reflection of the fact that there is no clear first minimum in the scattering profile.

As mentioned above, one important assumption to obtain N_{agg} is that the micelle core is free of solvent. It was previously reported that the amount of solvent in the micelle core is mainly dictated by the distance of the experimental temperature to the critical micelle temperature (CMT);[44,45] when this distance is sufficiently large, the solvent fraction in the core approaches zero. According to experimental results on PS-*b*-PI in diethyl phthalate (DEP) and dibutyl phthalate (DBP), which are solvents selective to the polystyrene block, this temperature interval is approximately 40−70 °C. A similar conclusion was drawn by Liu et al. in a study of an LCST system, PEO-*b*-PPO-*b*-PEO in water, who noted that as the temperature was increased further above the CMT, the solvent fraction in the core became lower.[46] In the current study, the experimental temperature (60 °C) is ∼80 °C above the highest CMT of all the seven copolymers (see Figure S3 in the Supporting Information), and therefore the assumption of negligible solvent penetration is justified. We can also consider this issue in terms of the magnitude of χ. Seitz et al. have calculated by self-consistent field theory that when $\chi_{solvent\text{-}core}$ increases from 0.7 to 1.1, the solvent fraction in the micelle core (φ_s) decreases dramatically from 0.6 to 0.25.[47] Although the χ between PnBMA and [EMIM][TFSI] has not been measured directly, Hoarfrost et al. measured the χ between PnBMA and mixtures of [EMIM][TFSI] and [BMIM][TFSI].[48] By extrapolating the [BMIM][TFSI] wt % to zero, we estimate that $\chi_{PnBMA/EMIM} \approx 1.4$ at 60 °C. This is quite a large χ, under which the solvent fraction in micelle core should be almost nil.

Figure 3a shows the dependence of R_c on the number of repeat units in the core block, N_B, in which the slope for the six larger polymers is determined to be 0.71 ± 0.01. This relationship is in rough agreement with Halperin's scaling theory, which predicts R_c to be proportional to $N_B^{0.60-0.67}$.[7] The exponent obtained from this experiment is slightly larger than that predicted for either the crew-cut or hairy limits. More elaborate theories have included an additional logarithmic term in the free energy of the corona block, which contributes to the size of the micelle core as well. Zhulina and co-workers proposed that in the hairy micelle limit, $R_c \sim N_B^{3/5}K^{-2/5}$, in which $K \sim \ln(N_B^{-11/15}N_A)$ when the solvent is good for the corona block ($\nu = 3/5$).[6,49,50] As $K^{-2/5}$ increases with N_B, therefore, the net scaling exponent between R_c and N_B should be greater than 3/5. Nagarajan and Ganesh found a relationship ($R_c \sim N_B^{0.70-0.73}$) by calculations for PS-*b*-PB/heptane and PEO-*b*-PPO/water systems using mean-field theory,[9] in excellent agreement with our experimental result. In their calculation, the three essential parameters ($\chi_{solvent\text{-}core}$, $\chi_{solvent\text{-}corona}$, and $\gamma_{solvent\text{-}core}$) are rationalized based on literature data for real systems, and aspects of their predictions are corroborated by experimental data for PS-*b*-PI in heptane

DOI: 10.1021/acs.macromol.6b00315
Macromolecules XXXX, XXX, XXX−XXX

conducted by Bahadur et al.,[28] with reasonable comparison between theory and the experiment.

On the basis of the fitting results, the interfacial widths in all the seven micelle specimens are below 1 nm, thus negligible compared to both R_c and L_{corona}; therefore, the corona thickness, L_{corona}, can be estimated as the difference between R_h obtained by DLS and R_c obtained by SAXS. Interestingly, for this system L_{corona} shows little dependence on N_B ($L_{corona} \sim N_B^{-0.04\pm0.05}$) as shown in Figure 3b, which deviates from the relationship $L_{corona} \sim N_B^{0.16-0.20}$ anticipated by the scaling theory. However, the scaling theory in the hairy limit assumes $R_c \ll L$, while in our experiments the micelles all have more comparable core and corona sizes, and which therefore fall between the two limiting cases. In fact, either limit is difficult to access experimentally, at least in uncharged systems. Zhulina et al. studied this intermediate case and found that $L_{corona} \sim N_A^{9/11} N_B^{0}$, assuming a good solvent for the corona, which indicates that L_{corona} is independent of N_B.[6,50] Nagarajan and Ganesh also gave $L_{corona} \sim N_B^{0.06-0.07} N_A^{0.68-0.74}$ in their mean-field study,[9] implying a much weaker dependence on N_B than the scaling theory, and very close to our result.

We can compare the mean square end-to-end distance of the core block $\sqrt{\langle R_0^2 \rangle}$ ($=(Nb^2)^{1/2}$) with the micelle core radius R_c. Since the statistical segment length (b) of PnBMA is 6.1 Å,[51] therefore, $\sqrt{\langle R_0^2 \rangle}$ of the PnBMA block of PMMA-*b*-PnBMA (25−13), (25−24), (25−31), (25−35), (25−44), (25−53), and (25−78) are estimated to be 59, 79, 90, 96, 107, 118, and 143 Å, respectively. On the basis of the results in Table 3, R_c of these micelles are approximately 1−1.5 times as large as $\sqrt{\langle R_0^2 \rangle}$, indicating significant stretching of the core block. This is not only due to the geometrical restriction, but also due to the crowding on the tethered interface. Note that in a sphere, only one chain needs to reach the center of the core, so to have the core radius significantly larger than the unperturbed end-to-end distance is proof of the importance of chain stretching. This reflects the fact that the micelles tend to increase N_{agg} in order to diminish the surface area per chain, and thus the interface free energy, which also agrees with the aforementioned theories.

An important question that needs to be addressed is whether or not these PMMA-*b*-PnBMA micelles are at equilibrium under the experimental conditions. It is well-known that nonergodicity occurs widely in macromolecular micelle systems, which is not only attributed to the glassy cores, but also to geologically slow chain exchange caused by high incompatibility between the core and the solvent.[52−57] In our experiment, the micelles are at equilibrium when they are initially formed in the presence of cosolvent; however, as the methylene chloride is further evaporated, the interfacial tension between the solvent and the core increases, and thus the equilibrium aggregation number should also increase. Under such circumstances, the micelles may no longer be at equilibrium when in the pure ionic liquid, as the number of micelles has to decrease, either by chain exchange or by coalescence. According to our preliminary results on micelle chain exchange in this system, only the two samples with the shortest PnBMA blocks have appreciable chain exchange rate at ∼60 °C;[58] even this does not guarantee that these two micelle samples are fully equilibrated, since the rearrangement process requires a change in N_{agg}, which is a much slower process than single chain exchange according to Aniansson−Wall theory.[59−61] Accordingly, we infer that these micelles reflect the equilibrium state achieved when the micelles were first formed, and not the equilibrium state in the pure ionic liquid. However, the application of equilibrium theory is still justified, given that all the micelles were formed under equivalent conditions.

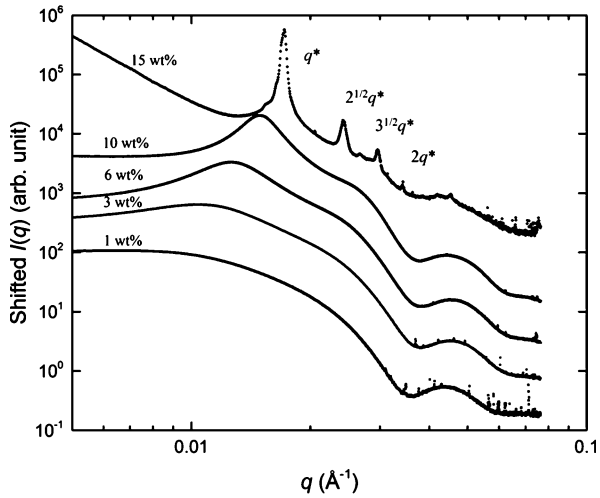

Figure 4. SAXS profiles of PMMA-*b*-PnBMA (25−35) in [EMIM]-[TFSI] at various concentrations at 60 °C. The profiles are shifted vertically by factors of 3 for clarity.

The scattering profiles of PMMA-*b*-PnBMA (25−35) micelles at higher concentration are shown in Figure 4. At 1 wt % concentration, the scattering profile does not show structure factor peaks; however, starting from 3 wt %, a structure peak emerges at low q, which progressively evolves into well-defined Bragg peaks at 15 wt % copolymer. The $q/q^* = 1{:}2^{1/2}{:}3^{1/2}{:}2$ pattern ($q^* \approx 0.017$ Å) strongly suggests a body-centered cubic (BCC) packing, as is often observed when the concentration of spherical micelles exceeds the critical overlap concentration.[34,44,62] However, due to the absence of characteristic peaks at higher q, the possibility of simple cubic packing cannot be ruled out. Nevertheless, assuming a BCC lattice, the nearest neighbor radius (R_{nn}) between the two micelles can be calculated from the BCC lattice parameter (a_{bcc}):

$$R_{nn} = \frac{\sqrt{6}}{4}\frac{2\pi}{q^*} = \frac{\sqrt{3}}{4}a_{bcc} \tag{4}$$

At 15 wt % copolymer concentration, R_{nn} = 224 Å, slightly smaller than the R_h of the same micelle (240 Å) in 1 wt % solution. This presumably reflects some interpenetration of the corona chains at high concentration.

At 15 wt % copolymer concentration, R_{nn} = 224 Å, slightly smaller than the R_h of the same micelle (240 Å) in 1 wt % solution. This presumably reflects some interpenetration of the corona chains at high concentration.

■ SUMMARY

In this report, we quantified the structure of seven poly(methyl methacrylate-*b*-*n*-butyl methacrylate) (PMMA-*b*-PnBMA) diblock copolymers in [EMIM][TFSI]; the corona block was fixed, and the core block length was varied. The micelle hydrodynamic radii R_h were determined by DLS using cumulant fitting, and the corresponding core radii R_c were extracted from SAXS data through fitting to the Pedersen

DOI: 10.1021/acs.macromol.6b00315
Macromolecules XXXX, XXX, XXX−XXX

model. This allowed for a precise determination of the dependence of R_c and L_{corona} on the degree of polymerization of the core block, N_B: $R_c \sim N_B^{0.71\pm0.01}$ and $L_{corona} \sim N_B^{-0.04\pm0.05}$. These results are in excellent agreement with the mean-field calculations of Nagarajan and Ganesh,[9,10] but they are only approximately consistent with scaling theory in the hairy micelle limit ($L \gg R_c$). This may be due in part to the comparable dimensions of the core and corona. The experimental results suggest that the core blocks are significantly stretched in the micelle. In addition, in the case of higher copolymer concentrations, micelles tend to pack onto a BCC lattice. Overall, this work provides a thorough and quantitative test of theories of micelle dimensions and will also aid in the ongoing study of the kinetics of chain exchange between micelles, an unresolved fundamental issue in polymer physics.

■ APPENDIX

Fitting Model for SAXS Data

The scattering form factor of a single micelle with a spherical core and Gaussian corona chains contains four terms: the self-correlation of the core, the self-correlation of the chains, the cross-term between the core and chains, and the cross-term between different chains.[42] The equation can be written as

$$P_{mic}(q) = N_{agg}{}^2\beta_{core}{}^2A_{core}{}^2(q) + N_{agg}\beta_{corona}{}^2P_{chain}(q) + 2N_{agg}{}^2\beta_{core}\beta_{corona}A_{core}(q)A_{corona}(q) + N_{agg}(N_{agg} - 1)\beta_{corona}{}^2A_{corona}{}^2(q) \quad \text{(A1)}$$

in which q, N_{agg}, β_{core} and β_{corona} are the scattering vector, aggregation number, total excess scattering length of the core block, and total excess scattering length of the corona block, respectively. By definition, $\beta_{core} = (\rho_{core} - \rho_{sol})v_{core\text{-}block}$ and $\beta_{corona} = (\rho_{corona} - \rho_{sol})v_{corona\text{-}block}$, where ρ_{core}, ρ_{corona} and ρ_{sol} are the scattering length densities of the core block, corona block and solvent, respectively; $v_{core\text{-}block}$ and $v_{corona\text{-}block}$ are the volumes of one core chain and one corona chain, respectively.

In the first term, for a spherical core with radius R_c and core−corona interface thickness σ_{int}, $A_{core}{}^2(q)$ can be written as

$$A_{core}^2(q) = \Phi^2(qR_c)\exp(-q^2\sigma_{int}^2) \quad \text{(A2)}$$

where $\Phi(x) = 3(\sin x - x\cos x)/x^3$ is the form factor amplitude of a sphere with a sharp interface. The last exponential term takes into account the "fuzziness" of the interface between core and corona domains.

The second term reflects the correlation between two monomers in the same Gaussian chain, therefore, $P_{chain}(q)$ adapts the form of the Debye function:

$$P_{chain}(q) = \frac{2[\exp(-q^2R_g{}^2) - 1 + q^2R_g{}^2]}{q^4R_g{}^4} \quad \text{(A3)}$$

where R_g is the radius of gyration of the corona chains.

The last two terms both contain the contribution of corona scattering. The form factor of the corona chains is given as the normalized Fourier transform of the average radial density distribution of the micelle corona, $\rho_{corona}(r)$:

$$A_{corona}(q) = \frac{4\pi\int\rho_{corona}(r)\frac{\sin(qr)}{qr}r^2\,dr}{4\pi\int\rho_{corona}(r)r^2\,dr}\exp(-q^2\sigma_{int}{}^2/2) \quad \text{(A4)}$$

In this work, a linear combination of two partial cubic b spline functions are used as the $\rho_{corona}(r)$, as has been described by Pedersen et al.[43]

In a real system, the polydispersity of the micelle size also has to be taken into account, in which a Gaussian distribution is assumed for the core radius, while the corona chain size (R_g) and the thickness of core−corona interface (σ_{int}) can be seen as constants. Under this assumption

$$D(R_c) = \frac{1}{\sqrt{2\pi}\sigma_R}\exp\left[-\frac{(R_c - \langle R_c\rangle)^2}{2\sigma_R{}^2}\right] \quad \text{(A5)}$$

in which $\langle R_c\rangle$ is the average core radius and σ_R is the standard deviation of the core radius. The total scattering intensity now can be written as the following equation:

$$I(q) = \int D(R_c)P_{mic}(q)\,dR_c \quad \text{(A6)}$$

Overall, there are seven adjustable parameters in this model: the average micelle core radius (R_c), the aggregation number (N_{agg}), the core−corona interface thickness (σ_{int}), radius of gyration of the corona chains (R_g), standard deviation of the core radius (σ_R), as well as the two fitting parameters (a_1, s) in the $\rho_{corona}(r)$ term. The other five parameters, the core block volume ($v_{core\text{-}block}$), the corona block volume ($v_{corona\text{-}block}$), and the scattering length density of the core (ρ_{core}), corona (ρ_{corona}) and solvent (ρ_{sol}), are fixed. Additionally, an arbitrary prefactor is multiplied to the total scattering intensity, $I(q)$, because the SAXS data were not reduced to an absolute scale. The complete Pedersen model with structure factor can be found in refs 34 and 43.

■ ASSOCIATED CONTENT

Supporting Information

The Supporting Information is available free of charge on the ACS Publications website at DOI: 10.1021/acs.macromol.6b00315.

^{1}H NMR spectra and SEC traces of the seven block copolymers, CMT of the block copolymers, DLS and SAXS data at various temperatures, and comparison between the two fitting methods (Figures S1 − S6 and Table S1) (PDF)

■ AUTHOR INFORMATION

Corresponding Author

*(T.P.L.) E-mail: lodge@umn.edu.

Notes

The authors declare no competing financial interest.

■ ACKNOWLEDGMENTS

This work was supported by the National Science Foundation (NSF) through Award DMR-1206459. The SAXS experiments were conducted on the DuPont−Northwestern−Dow Collaborative Access Team (DND-CAT) Synchrotron Research Center located at Sector 5 of the Advanced Photon Source. DND-CAT is supported by E. I. DuPont de Nemours & Co., Dow Chemical Company, the U.S. National Science Foundation through Grant DMR-9304725, and the State of Illinois through the Department of Commerce and the Board of Higher Education Grant IBHE HECA NWU 96. Use of the Advanced Photon Source was supported by the U.S. Depart-

DOI: 10.1021/acs.macromol.6b00315
Macromolecules XXXX, XXX, XXX−XXX

ment of Energy, Basic Energy Sciences, Office of Science, under Contract No. W-31-109-Eng-38.

REFERENCES

(1) de Gennes, P.-G. Macromolecules and Liquid Crystals: Reflections on Certain Lines of Research. In *Solid State Physics*; Liebert, J., Ed.; Academic: New York, 1978; Suppl. 14, pp 9−11.

(2) Daoud, M.; Cotton, J. P. Star shaped polymers: a model for the conformation and its concentration dependence. *J. Phys. (Paris)* **1982**, *43*, 531−538.

(3) Leibler, L.; Orland, H.; Wheeler, J. C. Theory of critical micelle concentration for solutions of block copolymers. *J. Chem. Phys.* **1983**, *79*, 3550−3557.

(4) Noolandi, J.; Hong, K. M. Interfacial properties of immiscible homopolymer blends in the presence of block copolymers. *Macromolecules* **1982**, *15*, 482−492.

(5) Noolandi, J.; Hong, K. M. Theory of block copolymer micelles in solution. *Macromolecules* **1983**, *16*, 1443−1448.

(6) Zhulina, E. B.; Birshtein, T. M. Conformations of molecules of block copolymers in selective solvents (micellar structures). *Polym. Sci. U.S.S.R.* **1985**, *27*, 570−578.

(7) Halperin, A. Polymeric micelles: a star model. *Macromolecules* **1987**, *20*, 2943−2946.

(8) Halperin, A.; Tirrell, M.; Lodge, T. P. Tethered chains in polymer microstructures. *Adv. Polym. Sci.* **1992**, *100*, 31−71.

(9) Nagarajan, R.; Ganesh, K. Block copolymer self-assembly in selective solvents: Spherical micelles with segregated cores. *J. Chem. Phys.* **1989**, *90*, 5843−5856.

(10) Nagarajan, R.; Ganesh, K. Solubilization in spherical block copolymer micelles: Scaling analysis based on star model. *J. Chem. Phys.* **1993**, *98*, 7440−7450.

(11) Binder, K. *Monte Carlo and molecular dynamics simulations in polymer science*; Oxford University Press: New York, 1995.

(12) Milchev, A.; Bhattacharya, A.; Binder, K. Formation of Block Copolymer Micelles in Solution: A Monte Carlo Study of Chain Length Dependence. *Macromolecules* **2001**, *34*, 1881−1893.

(13) Kim, S. H.; Jo, W. H. A Monte Carlo simulation for the micellization of ABA- and BAB-type triblock copolymers in a selective solvent. II. Effects of the block composition. *J. Chem. Phys.* **2002**, *117*, 8565−8572.

(14) Riess, G. Micellization of block copolymers. *Prog. Polym. Sci.* **2003**, *28*, 1107−1170.

(15) Zhulina, E. B.; Borisov, O. V. Theory of Block Polymer Micelles: Recent Advances and Current Challenges. *Macromolecules* **2012**, *45*, 4429−4440.

(16) Kotaka, T.; Tanaka, T.; Hattori, M.; Inagaki, H. Block Copolymer Micelles in Dilute Solution. *Macromolecules* **1978**, *11*, 138−145.

(17) Bluhm, T. L.; Whitmore, M. D. Styrene/butadiene block copolymer micelles in heptane. *Can. J. Chem.* **1985**, *63*, 249−252.

(18) Bluhm, T. L.; Malhotra, S. L. Poly(styrene-b-isoprene) micelles. Effect of molecular weight on micelle size. *Eur. Polym. J.* **1986**, *22*, 249−251.

(19) Oranli, L.; Bahadur, P.; Riess, G. Hydrodynamic studies on micellar solutions of styrene−butadiene block copolymers in selective solvents. *Can. J. Chem.* **1985**, *63*, 2691−2696.

(20) Xu, R.; Winnik, M. A.; Hallett, F. R.; Riess, G.; Croucher, M. D. Light-scattering study of the association behavior of styrene-ethylene oxide block copolymers in aqueous solution. *Macromolecules* **1991**, *24*, 87−93.

(21) Xu, R.; Winnik, M. A.; Riess, G.; Chu, B.; Croucher, M. D. Micellization of polystyrene-poly(ethylene oxide) block copolymers in water. 5. A test of the star and mean-field models. *Macromolecules* **1992**, *25*, 644−652.

(22) Antonietti, M.; Heinz, S.; Schmidt, M.; Rosenauer, C. Determination of the Micelle Architecture of Polystyrene/Poly(4-vinylpyridine) Block Copolymers in Dilute Solution. *Macromolecules* **1994**, *27*, 3276−3281.

(23) Calderara, F.; Hruska, Z.; Hurtrez, G.; Lerch, J. P.; Nugay, T.; Riess, G. Investigation of Polystyrene-Poly(ethylene oxide) Block Copolymer Micelle Formation in Organic and Aqueous Solutions by Nonradiative Energy Transfer Experiments. *Macromolecules* **1994**, *27*, 1210−1215.

(24) Jada, A.; Hurtrez, G.; Siffert, B.; Riess, G. Structure of polystyrene-block-poly(ethy1ene oxide) diblock copolymer micelles in water. *Macromol. Chem. Phys.* **1996**, *197*, 3697−3710.

(25) Förster, S.; Zisenis, M.; Wenz, E.; Antonietti, M. Micellization of strongly segregated block copolymers. *J. Chem. Phys.* **1996**, *104*, 9956−9970.

(26) Tao, J.; Stewart, S.; Liu, G.; Yang, M. Star and Cylindrical Micelles of Polystyrene-block-poly(2-cinnamoylethyl methacrylate) in Cyclopentane. *Macromolecules* **1997**, *30*, 2738−2745.

(27) Pitsikalis, M.; Siakali-Kioulafa, E.; Hadjichristidis, N. Block Copolymers of Styrene and Stearyl Methacrylate. Synthesis and Micellization Properties in Selective Solvents. *Macromolecules* **2000**, *33*, 5460−5469.

(28) Bahadur, P.; Sastry, N. V.; Marti, S.; Riess, G. Micellar behaviour of styrene-isoprene block copolymers in selective solvents. *Colloids Surf.* **1985**, *16*, 337−346.

(29) Jada, A.; Siffert, B.; Riess, G. Adsorption at the solid-solution interface and micelle formation in water of the poly(oxyethylene-styrene-oxyethylene) triblock copolymer. *Colloids Surf., A* **1993**, *75*, 203−209.

(30) Quintana, J. R.; Salazar, R. A.; Katime, I. Micelle formation and polyisobutylene solubilization by polystyrene-block-poly(ethylene-co-butylene)-block-polystyrene block copolymers. *Macromol. Chem. Phys.* **1995**, *196*, 1625−1634.

(31) Pitsikalis, M.; Siakali-Kioulafa, E.; Hadjichristidis, N. Block copolymers of styrene and n-alkyl methacrylates with long alkyl groups. Micellization behavior in selective solvents. *J. Polym. Sci., Part A: Polym. Chem.* **2004**, *42*, 4177−4188.

(32) Guerrero-Sanchez, C.; Wouters, D.; Fustin, C.-A.; Gohy, J.-F.; Lohmeijer, B. G. G.; Schubert, U. S. Structure-Property Study of Diblock Copolymer Micelles: Core and Corona Radius with Varying Composition and Degree of Polymerization. *Macromolecules* **2005**, *38*, 10185−10191.

(33) LaRue, I.; Adam, M.; Zhulina, E. B.; Rubinstein, M.; Pitsikalis, M.; Hadjichristidis, N.; Ivanov, D. A.; Gearba, R. I.; Anokhin, D. V.; Sheiko, S. S. Effect of the Soluble Block Size on Spherical Diblock Copolymer Micelles. *Macromolecules* **2008**, *41*, 6555−6563.

(34) Choi, S.; Bates, F. S.; Lodge, T. P. Structure of Poly(styrene-b-ethylene-alt-propylene) Diblock Copolymer Micelles in Squalane. *J. Phys. Chem. B* **2009**, *113*, 13840−13848.

(35) Jensen, G. V.; Shi, Q.; Deen, G. R.; Almdal, K.; Pedersen, J. S. Structures of PEP−PEO Block Copolymer Micelles: Effects of Changing Solvent and PEO Length and Comparison to a Thermodynamic Model. *Macromolecules* **2012**, *45*, 430−440.

(36) Zinn, T.; Willner, L.; Lund, R.; Pipich, V.; Appavou, M.; Richter, D. Surfactant or block copolymer micelles? Structural properties of a series of well-defined n-alkyl-PEO micelles in water studied by SANS. *Soft Matter* **2014**, *10*, 5212−5220.

(37) Wiley, R. H.; Brauer, G. M. Refractometric Determination of Second-Order Transition Temperatures in Polymers. 11. Some Acrylic, Vinyl Halide, and Styrene Polymers. *J. Polym. Sci.* **1948**, *3*, 455.

(38) Bonhôte, P.; Dias, A.-P.; Papageorgiou, N.; Kalyanasundaram, K.; Grätzel, M. Hydrophobic, Highly Conductive Ambient-Temperature Molten Salts. *Inorg. Chem.* **1996**, *35*, 1168−1178.

(39) Numasawa, N.; Hamada, T.; Nose, T. Static properties of polystyrene in poly(methyl methacrylate)−benzene semidilute solution. *J. Polym. Sci., Polym. Lett. Ed.* **1985**, *23*, 1−4.

(40) Jakeš, J. Regularized Positive Exponential Sum (REPES) Program - A Way of Inverting Laplace Transform Data Obtained by Dynamic Light Scattering. *Collect. Czech. Chem. Commun.* **1995**, *60*, 1781−1797.

(41) Koppel, D. E. Analysis of Macromolecular Polydispersity in Intensity Correlation Spectroscopy: The Method of Cumulants. *J. Chem. Phys.* **1972**, *57*, 4814−4820.

DOI: 10.1021/acs.macromol.6b00315
Macromolecules XXXX, XXX, XXX−XXX

(42) Pedersen, J. S.; Svaneborg, C.; Almdal, K.; Hamley, I. W.; Young, R. N. A Small-Angle Neutron and X-ray Contrast Variation Scattering Study of the Structure of Block Copolymer Micelles: Corona Shape and Excluded Volume Interactions. *Macromolecules* **2003**, *36*, 416−433.
(43) Castelletto, V.; Hamley, I. W.; Pedersen, J. S. A small-angle neutron scattering investigation of the structure of highly swollen block copolymer micelles. *J. Chem. Phys.* **2002**, *117*, 8124−8129.
(44) Bang, J.; Viswanathan, K.; Lodge, T. P.; Park, M. J.; Char, K. Temperature-dependent micellar structures in poly(styrene-b-isoprene) diblock copolymer solutions near the critical micelle temperature. *J. Chem. Phys.* **2004**, *121*, 11489−11500.
(45) Lodge, T. P.; Xu, X.; Ryu, C. Y.; Hamley, I. W.; Fairclough, J. P. A.; Ryan, A. J.; Pedersen, J. S. Structure and Dynamics of Concentrated Solutions of Asymmetric Block Copolymers in Slightly Selective Solvents. *Macromolecules* **1996**, *29*, 5955−5964.
(46) Liu, Y.; Chen, S.-H.; Huang, J. S. Small-Angle Neutron Scattering Analysis of the Structure and Interaction of Triblock Copolymer Micelles in Aqueous Solution. *Macromolecules* **1998**, *31*, 2236−2244.
(47) Seitz, M. E.; Burghardt, W. R.; Shull, K. R. Micelle Morphology and Mechanical Response of Triblock Gels. *Macromolecules* **2009**, *42*, 9133−9140.
(48) Hoarfrost, M. L.; He, Y.; Lodge, T. P. Lower Critical Solution Temperature Phase Behavior of Poly(n-butyl methacrylate) in Ionic Liquid Mixtures. *Macromolecules* **2013**, *46*, 9464−9472.
(49) Birshtein, T. M.; Zhulina, E. B. Scaling theory of supermolecular structures in block copolymer-solvent systems: 1. Model of micellar structures. *Polymer* **1989**, *30*, 170−177.
(50) Zhulina, E. B.; Adam, M.; LaRue, I.; Sheiko, S. S.; Rubinstein, M. Diblock Copolymer Micelles in a Dilute Solution. *Macromolecules* **2005**, *38*, 5330−5351.
(51) Helfand, E.; Sapse, A. M. Theory of unsymmetric polymer-polymer interfaces. *J. Chem. Phys.* **1975**, *62*, 1327−1331.
(52) Won, Y.-Y.; Davis, H. T.; Bates, F. S. Molecular Exchange in PEO−PB Micelles in Water. *Macromolecules* **2003**, *36*, 953−955.
(53) Lund, R.; Willner, L.; Stellbrink, J.; Lindner, P.; Richter, D. Logarithmic Chain-Exchange Kinetics of Diblock Copolymer Micelles. *Phys. Rev. Lett.* **2006**, *96*, 068302.
(54) Lund, R.; Willner, L.; Lindner, P.; Richter, D. Structural Properties of Weakly Segregated PS−PB Block Copolymer Micelles in n-Alkanes: Solvent Entropy Effects. *Macromolecules* **2009**, *42*, 2686−2695.
(55) Choi, S.-H.; Bates, F. S.; Lodge, T. P. Molecular Exchange in Ordered Diblock Copolymer Micelles. *Macromolecules* **2011**, *44*, 3594−3604.
(56) Lu, J.; Bates, F. S.; Lodge, T. P. Chain Exchange in Binary Copolymer Micelles at Equilibrium: Confirmation of the Independent Chain Hypothesis. *ACS Macro Lett.* **2013**, *2*, 451−455.
(57) Lu, J.; Bates, F. S.; Lodge, T. P. Remarkable Effect of Molecular Architecture on Chain Exchange in Triblock Copolymer Micelles. *Macromolecules* **2015**, *48*, 2667−2676.
(58) Ma, Y.; Lodge, T. P. Unpublished results.
(59) Aniansson, E. A. G.; Wall, S. N.; Almgren, M.; Hoffmann, H.; Kielmann, I.; Ulbricht, W.; Zana, R.; Lang, J.; Tondre, C. Theory of the kinetics of micellar equilibria and quantitative interpretation of chemical relaxation studies of micellar solutions of ionic surfactants. *J. Phys. Chem.* **1976**, *80*, 905−922.
(60) Cavicchi, K. A.; Lodge, T. P. Self-Diffusion and Tracer Diffusion in Sphere-Forming Block Copolymers. *Macromolecules* **2003**, *36*, 7158−7164.
(61) Meli, L.; Santiago, J. M.; Lodge, T. P. Path-Dependent Morphology and Relaxation Kinetics of Highly Amphiphilic Diblock Copolymer Micelles in Ionic Liquids. *Macromolecules* **2010**, *43*, 2018−2027.
(62) McConnell, G. A.; Gast, A. P.; Huang, J. S.; Smith, S. D. Disorder-order transitions in soft sphere polymer micelles. *Phys. Rev. Lett.* **1993**, *71*, 2102−2105.

DOI: 10.1021/acs.macromol.6b00315
Macromolecules XXXX, XXX, XXX−XXX